ON THE INFLUENCE OF CHANGING SNOW PROPERTIES ONTO THE STRUCTURAL BEHAVIOUR OF A SNOWBOARD UNDERGOING A CARVED TURN

Benoit Caillaud[1,*], Johannes Gerstmayr[1]

[1] *Institute of Mechatronics, University of Innsbruck, Austria*

ABSTRACT: The purpose of this study was to numerically investigate the influence of different snow conditions onto the structural behaviour of a snowboard undergoing the conditions of a carved turn. The properties of different types of snow were numerically idealized and the deformations and pressure distribution along the contact edge of a snowboard were observed, in an attempt to understand their sensitivity to the environmental parameters. A static load bench was developed in-house and a simplified snowboard prototype was manufactured in order to represent the in-situ conditions. The experimental set-up was idealized in a finite element model, representing the composite structure and its loading environment. A method for the validation of the numerical model was proposed, based on the comparison of the experimental and numerical displacement fields, and consisted in a best-fit algorithm to superimpose both deformed shapes. The congruence between the two deformed surfaces was expressed with statistical means, and constituted the target function for optimization frameworks. Additionally, the contact pressure at the interface was experimentally assessed with the use of pressure measurement tape, and compared with the numerical predictions. The results of the finite element simulation were then explored to give an insight on the influence of the snow properties onto the structural behaviour.

Keywords: snowboarding, carving turn, FEM, test validation, contact pressure.

1. INTRODUCTION

State of the art of the development of snowboard structures is mostly using the experience of the manufacturers, the subjective feedback from in-situ tests including several years of try and error. Consequent research has been made to characterize ski/snowboard structures (Nordt et al. (2016)) and their influence onto the behaviour on the snow (Federolf et al. (2016)). These approaches remain insufficient, since the deformed state of the structure (under given load state and environment conditions) is not considered during the design phase.

The present paper attempts to clarify how the geometry and the mechanical properties of a snowboard influence its behaviour under operation. Thus, a finite element model representing the conditions of a carved turn was developed and validated by comparing the deformations of a snowboard prototype with a full-scale test. The pressure distribution at the contact interface was observed. The coefficient of friction and contact stiffness at the interface were varied in order to simulate interactions with different types of snow. The numerical results were assessed in an attempt to gain understanding of the structural sensitivity to different snow properties.

*Corresponding author address:
Benoit Caillaud, Institute of Mechatronics, University of Innsbruck
Technikerstraße 13, 6020 Innsbruck;
tel: +43 512 507-62751
email: benoit.caillaud@student.uibk.ac.at

2. EXPERIMENTAL SET-UP

2.1. Static Load Bench

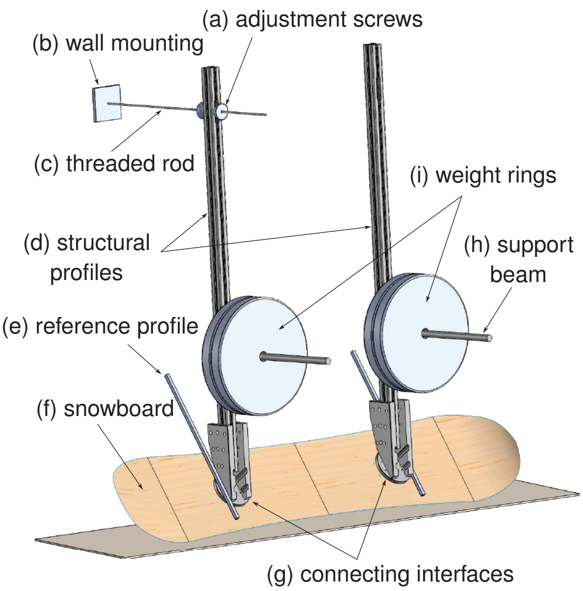

Figure 1: CAD model of the static load bench

The test bench developed in-house is represented in Figure 1. It consisted of two independent profiles (d) connected to the snowboard binding inserts via the connecting interfaces (g). Each profile was equipped with a support beam (h) that could be loaded with weight rings (i). The

position of the weight rings was adjusted along the support beams in order to bring the system on the desired tilt angle, ranging from $40°$ to $60°$. The contact took place between the snowboard and a rigid, flat aluminium plate. Once the weights were in position, the static equilibrium was sought by adjusting the angular position of the system with a threaded rod (c) and according adjustment screws (a). The system is statically determined when the equilibrium is reached, i.e. when the resultant of the reaction forces to the contact plate is aligned with the resultant of the total applied force. Thus, the threaded rod and adjustment screws are not transmitting any significant amount of load.
The input weight and the tilt angle could be adjusted independently for the front and rear bindings, and constitute the input parameters of the experiment.

The tested prototype consisted in a simplified snowboard structure manufactured according to the current industrial standards (Subic and Kovacs (2007)). The structure featured a 5.55 mm constant thickness core made out of two different types of wood (see Figure 3), sandwiched between two composite skins made out of epoxy reinforced fibreglass (each 0.665 mm thick). The snowboard geometry was defined as symmetric twin-tip and the sidecut had a constant radius of 7.05 m.

2.2. Measurement strategy

The Vicon motion tracking system was used to capture the deformed shape of the structure. The measurement process consisted in positioning 29 spherical retro-reflective markers (14 mm diameter) on the structure and measuring their position in space by triangulation, with the use of six Vero v2.2 cameras. The absolute positioning error of the Vicon system depends on the number of cameras and the visibility of the markers. For static measurements, it is reported to give an error of 0.15 mm (Merriaux et al. (2017)).

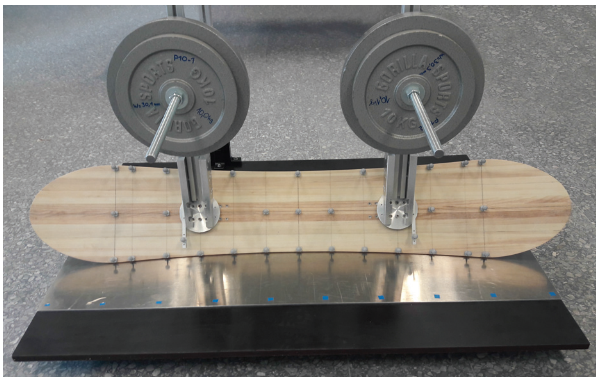

Figure 2: Front view of the load bench and the tested snowboard prototype equipped with 29 Vicon markers

Symmetrical loading conditions were defined on the static load bench. The total loading weight was equally split on both bindings and identically positioned, such that the tilt angles on both sides were as identical as possible. Twelve measurement sets were defined (Table 1) with different combinations of the total loading weight P (20, 40 and 60 kg) and tilt angles θ (ranging from $39°$ to 59°).

Table 1: Evaluation scheme. Twelve samples were defined with different combinations of the input weight (P) and tilt angles, reported for the rear binding (θ_R), front binding (θ_F) and the average over both values ($\bar{\theta}$)

set name	P [kg]	θ_R [°]	θ_F [°]	$\bar{\theta}$ [°]
A	60	54.5	54.0	54.3
B	60	49.7	49.7	49.7
C	60	43.5	44.0	43.8
D	60	39.0	39.3	39.2
E	40	41.9	42.2	42.1
F	40	46.3	46.4	46.4
G	40	51.7	52.0	51.9
H	40	57.1	57.4	57.3
I	20	59.3	59.2	59.3
J	20	54.3	54.3	54.3
K	20	49.7	50.0	49.9
L	20	45.8	46.0	45.9

2.3. Contact pressure

The contact pressure between the snowboard and the contact plate was experimentally determined with the use of a Prescale pressure measurement film, inserted during the measurement between the snowboard edge and the contact plane. The Prescale film used was composed of two polyester based sheets, one side containing a micro-encapsulated color-forming layer and the other side with a color-developing layer. When pressure is applied, the micro-capsules break and the color-developing material turns red, the intensity of the color varying with the applied pressure. The measurement errors of such films are reported to be approximately 10-15 percent for low contact pressure gradients (Hale and Brown (1992)).

The pressure range of the measurement film used was 2 to 10 MPa. The measurement was performed on the measurement set exhibiting the highest predicted contact pressure (set A), with the highest loading weight (60 kg) and tilt angle (54°).
The resulting coloured film was scanned and the color densities transcribed in the RGB24 color model. The color intensity was then compared to the given pressure scale and converted into actual pressure units (MPa). A smoothing spline was finally fitted through the measurement values and the pressure profile along the longitudinal direction could be estimated.

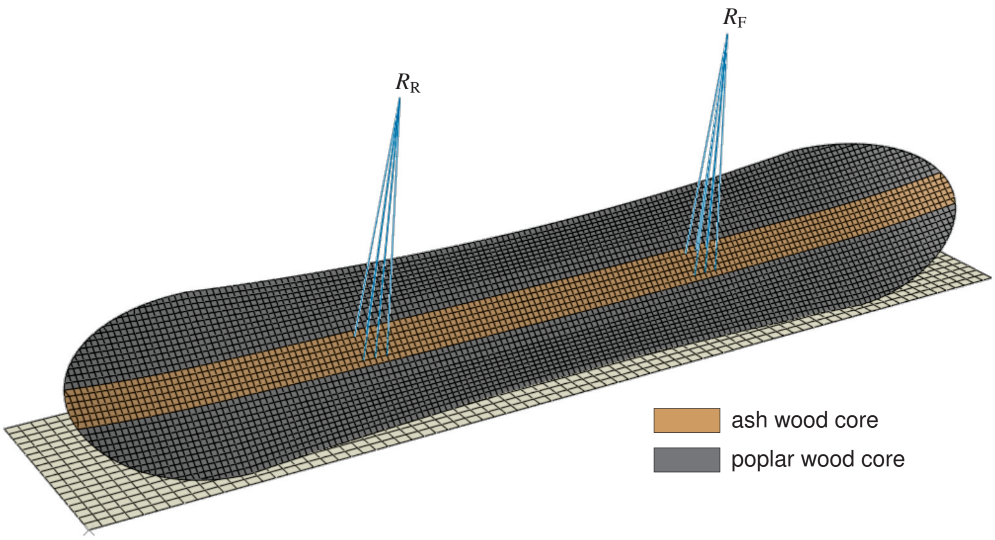

Figure 3: FE Model representation: the tilt angles and the loading weight are introduced via two reference nodes R_R and R_F, linked to the inserts locations via distributing couplings.

3. FINITE ELEMENT MODELLING

The snowboard prototype geometry and structure were idealized in a finite element model (FEM) representing the experimental conditions. Fully integrated finite-membrane-strain shell elements (3- and 4-nodes) were used to represent the structure, where composite shell sections were defined to represent each layer of the stacking independently within the elements. A rigid body plane was first introduced to simulate the experimental interaction with the contact plate. The contact formulation was defined as a hard contact pressure-overclosure interaction with a linear penalty stiffness, and a friction coefficient of 0.4 was introduced to simulate the interaction between the composite snowboard and the rigid aluminium plate.
In a second step, the contact plate stiffness, the coefficient of friction at the interface and the contact interaction formulation were varied in order to simulate interactions with different types of snow conditions (Gerling et al. (2017), Nachbauer et al. (2016)).

The mechanical properties of the materials used were evaluated in-house by laboratory testing and completed by additional literature references. The modulus of elasticity of ash and poplar woods as well as E-fiberglass/epoxy samples were statistically determined by three points bending testing on various samples. The values of the Poisson's ratios and shear modulus were extrapolated from Winandy (1994) for the wood samples, and from Schuermann (2007) for E-fiberglass/epoxy samples. The material properties used for the present investigation are reported in Table 2.

Table 2: Mechanical properties of the specimen investigated: elastic modulus (E_l longitudinal, E_t transversal), Poisson ratio (ν_{lt}), shear modulus (G_{lt})

Material	E_l [MPa]	E_t [MPa]	ν_{lt}	G_{lt} [MPa]
E-glass/epoxy	30510.	7845.	0.283	3220.
Ash wood	13000.	790.	0.420	810.
Poplar wood	8500.	575.	0.355	610.

A static stress analysis was performed considering geometrical nonlinearities. The loading was applied incrementally within each analysis step, where the nonlinear equilibrium equations were solved using Newton-Raphson iterations. Verification checks such as unit enforced displacement and rotation, stiffness equilibrium checks were performed to ensure that the FE model was mathematically accurate. The nodal displacements and the contact pressure at the interface were extracted from the analysis.

With an element size of approximatively $10 \times 10\,\mathrm{mm}$, the model contained 4 500 elements and over 30 000 degrees of freedom (DOFs). The analysis required in average approximatively 5 minutes to solve in the finite element software Abaqus® Academic Research release 6.13-2, on a 4-cores processor platform Intel® i7-6700 @3.40GHz and a maximum RAM memory of 16Gb.

4. RESULTS

4.1. *Assessment of deformation predictions*

For each measurement set, the experimental marker positions were interpolated into a polynomial surface, defined as the least square best fit of the measurements (Figure 4).

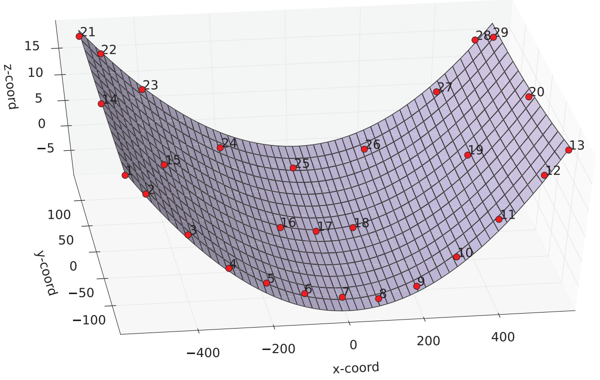

Figure 4: Polynomial surface interpolated from the experimental marker positions, measurement set A

The interpolated surface was used to superimpose the measured marker positions with the FE deformed surface, according to a least-square best-fit algorithm of the two point clouds (Ueyama (1991)). The direct comparison of the vertical positioning of the FE nodes cloud with the interpolated experimental surface reveals the quality of the fitting (Figure 5). The main differences occurred in the bindings areas subjected to high transverse deformations.

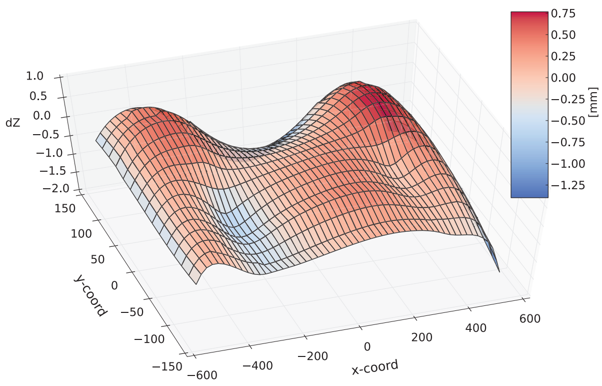

Figure 5: Vertical positioning differences between the deformed FEM and the interpolated surface of the marker positions, measurement set A

The validity of the numerical predictions was assessed by direct computing of the normal distances from the measured marker positions to the deformed FE model. The statistical distribution of the final absolute positioning differences is shown in (Figure 6) for the twelve measurement sets.

The experimental measurements of the global deformations were in good agreement with the numerical predictions. Over the twelve cases investigated, the mean positioning error of the experimental marker positions in comparison to the FE model was 0.559 mm, with 90% of the measurements below 1.200 mm and RMSE=0.720 mm. These results can be contrasted with the overall maximal longitudinal bending deflections of the snowboard, ranging from 15.7 mm to 32.5 mm. Taking into account the residual positioning errors due to the polynomial superimposition process, the final correlations appear to be satisfying.

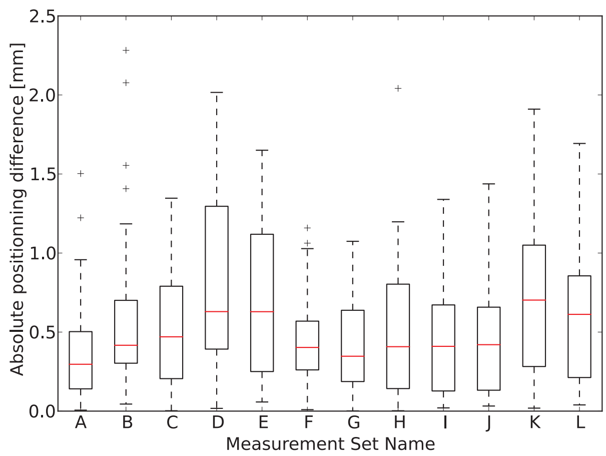

Figure 6: Final positioning differences between the experiment and the FEM deformed shapes - box plot representation for the twelve measurement sets

4.2. *Validation of the contact pressure*

The measurement of the contact pressure along the edge line of the snowboard was performed on the static load bench for the measurement set A. Although the minimum pressure of the Prescale film was 2.0 MPa, an interpolation could still be performed for lower red color levels down to a corresponding pressure value of about 1.0 MPa. For these low values however, the precision of the measurement is no longer guaranteed. The results exhibited four distinct locations, denoted as CPR (contact point fear area), BR (rear binding area), CPF (contact point front area), and BF (front binding area). The raw measurements are shown on Figure 7 together with the smoothing splines interpolations.

The maximum pressure measured on the CPR area was 4.43 MPa, and the maximum value in the BR area was 2.56 MPa (peak ratio of 1.7 for the rear location). The maximum pressure measured on the CPF area was 3.42 MPa, and the maximum value in the BF area was 2.16 MPa (peak ratio of 1.6 for the front location). The averaged contact pressure line was 1.1 mm wide at the contact points, and 0.7 mm wide at the binding locations. The linear pressure output from the FE model was converted in a surface pressure accordingly, and the results are

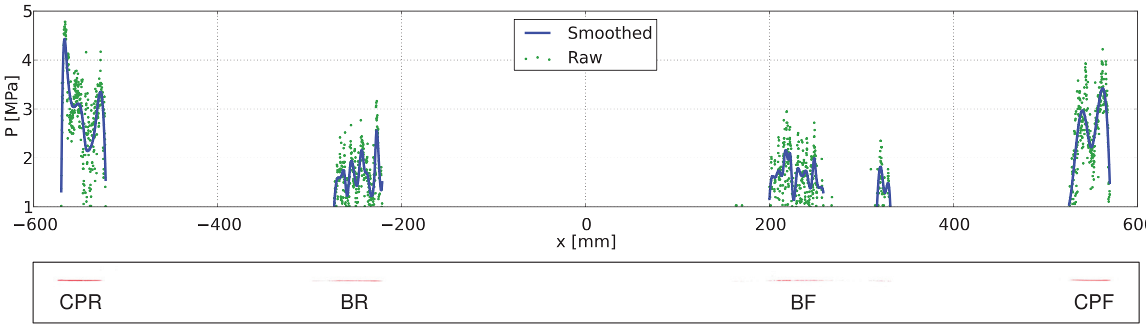

Figure 7: Experimental distribution of the contact pressure between the snowboard and the contact plate, for the measurement set A. The original red-colored Prescale film is shown below the chart, with the four distinct pressure locations: CPR, BR, BF and CPF

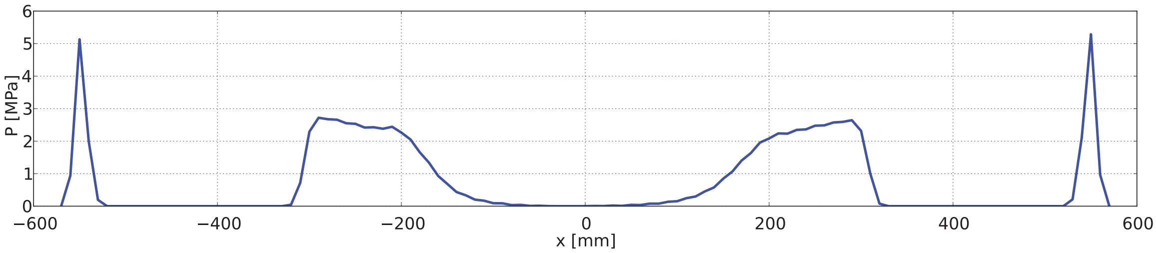

Figure 8: Numerical distribution of the contact pressure between the snowboard and the contact plate, measurement set A

shown in Figure 8. The maximum pressure computed in the CPR area was 5.13 MPa, and the maximum value in the BR area was 2.72 MPa (peak ratio of 1.9 for the rear location). The maximum pressure computed in the CPF area was 5.29 MPa, and the maximum value in the BF area was 2.64 MPa (peak ratio of 2.0 for the rear location).

4.3. Influence of snow properties

In order to determine the influence of different types of snow onto the structural behaviour, the elastic modulus of the contact plate was varied to represent the stiffness of various snow densities (Gerling et al. (2017)). The response of the snow to an input loading was defined by different pressure-overclosure interactions, simulating the snow resistance to penetration depth relationship. Additionally, the coefficient of friction between the snowboard and the contact surface was varied to simulate the corresponding interaction properties (Nachbauer et al. (2016)). The impact of the contact formulations onto the global deformations and the pressure distribution along the snowboard edge will be shown via the results of a sensitivity study framework.

5. CONCLUSION

The numerical representation of a simplified snowboard structure undergoing a carved turn has shown to be accurately representing the experimental setup. The validation of the finite element model showed that the simulation is suitable for predicting the structural deformations and the contact pressure at the interface with the external environment. The sensitivity of these output parameters was assessed against the modelling of different snow properties, and the results will be shown during the conference presentation.

REFERENCES

Doerner F., Koerblein C.H., Schindler C.H. (2014). On the accuracy of the pressure measurement film in Hertzian contact situations similar to wheel-rail contact applications. *Wear*, 317(1-2):241-245.

Federolf P., JeanRichard F., Fauve M., Lüthi A., Rhyner H., Dual J. (2005). Deformation of Snow During a Carved Ski Turn. *Cold Regions Science and Technology*, 46(1):69-77.

Gerling B., Löwe H., and Van Herwijnen A. (2017). Measuring the Elastic Modulus of Snow. *Geophysical Research Letters*, 44:11088–11096.

Hale J.E., Brown T.D. (1992). Contact stress gradient detection limits of Pressensor film. *Journal of Biomechanical Engineering*, 114:352-357.

Merriaux P., Dupuis Y., Boutteau R., Vasseur P. and Savatier X. (2017). A Study of Vicon System Positioning Performance. *Sensors*, 17(7):1591.

Nachbauer W., Kaps P., Hasler M., and Moessner M. (2016). Friction Between Ski and Snow. *The Engineering Approach to Winter Sports*, pp. 17-32.

A. Nordt, G. Springer and L. Kollar (1999). Computing the mechanical properties of alpine skis. *Sports Engineering*, 2(2):65-84.

Subic A., Kovacs J. (2007). Design and Materials in snowboarding. *Materials in Sports Equipment*, 2:192-200.

Schuermann H. (2007). Konstruieren mit Faser-Kunststoff-Verbunden. *Springer-Verlag, Berlin Heidelberg*, pp. 28-30.

Ueyama S. (1991). Least-Squares Estimation of Transformation Parameter Between Two Point Patterns. *IEEE Transactions on Pattern Analysis and Machine Intelligence*, 13(4):376-380.

Winandy J.E. (1994). Wood Properties. *Encyclopedia of Agricultural Science*, 4:549-561.